J Appl Electrochem (2013) 43:879–890
DOI 10.1007/s10800-013-0581-y

ORIGINAL PAPER

Seeding strategies for the deposition of high density network of nanoporous Au cluster catalyst on glassy carbon electrodes

M. Kamundi · L. Bromberg · P. Ogutu · N. Dimitrov

Received: 2 May 2013 / Accepted: 25 June 2013 / Published online: 9 July 2013

Abstract Recent developments demonstrated the feasibility of functionalized nanoporous Au (NPG) for application in catalysis. This work employed a variety of seeding strategies aimed at facilitating the synthesis of ultra-high density or nearly continuous cluster network on glassy carbon (GC) surfaces of quality and structure achievable on metal substrates only. The NPG synthetic process involving electrodeposition of $Au_xAg_{(1-x)}$ alloy and its subsequent de-alloying was performed on seeds generated by electrodeposition (Cu, Ag) and electroless (Pd, Au) approaches. The outcome of the densification process was assessed by electrochemical characterization and scanning electron microscopy. While some improvement was observed on Cu and Ag seeds, significantly higher nucleation density was obtained on Au-seeded GC surfaces where the deposit featured most typical de-alloying behavior leading to highest surface area evolution. The best overall quality of NPG film manifested by high density networks of overlapping, uniform, and very small clusters nearing structural continuity was achieved on Pd-seeded GC samples.

Keywords Glassy carbon · Seeding · Nanoporous gold · Catalysts · Electroless

1 Introduction

The drive toward efficient and durable fuel cells and metal–air batteries is founded on the development characterization and testing of a variety of catalysts based on nanoparticles [1, 2]. More recently, alternative approaches to synthesizing catalysts have been explored that use ultra thin layers of nanoporous metals [3, 4]. In a previous work, our group proposed a completely electrochemical scheme for fabricating a platinized nanoporous Au (Pt-NPG)-based catalyst for formic acid oxidation [4]. The synthetic protocol comprises electrochemical co-deposition of a $Au_xAg_{(1-x)}$ alloy, followed by selective electrochemical dissolution (de-alloying) of Ag. On metal substrates this protocol generates an ultrathin and continuous porous structure featuring a thickness of less than 20 nm. The final step rendering the NPG catalytically active involves functionalization with a layer of Pt no thicker than 1 nm. Accordingly synthesized catalysts were deposited on Au and glassy carbon (GC) electrodes and tested for activity and durability through formic acid oxidation [4]. Also, in more fundamentally oriented work these catalysts were studied in detail for structure, morphology, and surface area evolution [5]. The characterization results show general consistency of morphology and surface area evolution but reveal a major structural difference depending upon the carrier substrate. More specifically, continuous, smooth nanoporous deposits have been realized on Au and other metal substrates while largely isolated spherical clusters of various sizes result from deposition on GC [4]. Such clusters are normally a result of nucleation on energetically non-homogeneous and low-catalytic activity substrates [6]. The outcome of such scenario is a disperse nanocrystalline deposit that represents a network spatially localized clusters growing in three-dimensional (3D) mode right after their nucleation [6]. The latter constitute case an issue with the durability of the catalysts associated with generally poor adhesion to the GC surface and also with limited cluster-

M. Kamundi · L. Bromberg · P. Ogutu · N. Dimitrov (✉)
Department of Chemistry, State University of New York at Binghamton, PO Box 6000, Binghamton, NY 13902-6000, USA
e-mail: dimitrov@binghamton.edu

core accessibility to reagents in the catalytic process owing to inherently large particle size [4]. These drawbacks expectedly emphasize challenges with the quality, overall performance and/or durability of nanoporous metal (NPM)-based catalysts, especially when they are deposited on the most frequently used C-based supports.

In this work we address specifically this structural challenge by exploring extensively different means for substantial increase of the nucleation density upon initiation of the alloy deposition process. A higher nucleation density allows for distribution of the overall amount of alloy more evenly across the substrate resulting in a significantly thinner and preferably continuous layer. Approaches toward increasing the nucleation density could utilize electrodeposition-based pulse-plating scenarios and/or means for metallization of non-conductive materials especially for applications in the electronics industry [6]. While winning strategies for achieving high nucleation density by electrodeposition could be devised mainly based on the classical nucleation and growth arguments [6, 7], the electroless means could in some cases be more beneficial owing to less surface-selective nucleation on a variety of substrates. Featuring a remarkable diversity electroless approaches include metallization through the one-step process [8–10], the use of UV/VUV photo-induced decomposition on a deposited organo-palladium film [11, 12], use of H_2 RF plasma [13] for the reduction of a spin-coated thin copper formate film, the use of Cu(O) [10] species for seeding instead of Pd(O) species, pretreatment of SiO_2 and TiN substrates with $TiCl_4$ [14] molecules using repeated cyclic pulse and purge processes, etc. Most often non-conductors have been activated through the two-step process consisting of sensitization (Sn^{2+} ions) followed by activation (Pd(II) complex) in HCl media. That approach is applicable on glass [15, 16], plastics [16, 17], polyaniline films [18], modified nafion [17], Teflon [18], polymers [19], polyimides [20–22], e.g., Kapton polyimide film, etc.

In this exploratory work, an effort has been made to electrodeposit ultra thin and continuous alloy films on GC surfaces that would be comparable to those deposited on metal (Au). The entertained experimental approach relies on seeding of the GC with a dense ensemble of metal clusters that will facilitate the growth of a high density alloy cluster network that is prone to coalescence. The variety of seeding approaches of interest has been performed using electroless and electrodeposition metallization routines. The outcome of the densification process, representing the main objective of this work, has been assessed electrochemically throughout the synthetic process and by scanning electron microscopy (SEM) after completing the synthetic routine producing the NPG structure. The focus of the assessment has been on macro structure, surface coverage, cluster size, and overall surface area of the NPG layer. The compositional homogeneity and quality of mixing in the deposited alloy layers have been assessed by the de-alloying runs and the overall surface area evolution of the NPG structure after the de-alloying. This has been studied by Pb underpotential deposition (UPD) following characterization protocols described in our earlier work [23]. The surface area evolution has been cross-examined by H UPD measurements [24] carried out after platinization of accordingly developed NPG structures. The results obtained have been compared to those obtained on unseeded GC electrodes. Also, NPG layers generated by the proposed seeding approaches are critically compared vis-à-vis densification, uniformity, and developed surface area.

2 Experimental

2.1 Electrode preparation and potential referencing

Cylindrical glassy carbon working electrodes (Goodfellow, diameter 5 mm) were first mechanically polished down to 1 μm with alumina slurry on a Buehler polishing pad followed by rinsing and sonication for 5 min in a solution containing ethanol and *Barnstead Nanopure*® water ($R \geq 18.2$ MΩ cm). They were finally mechanically polished down to 0.05 μm with a diamond suspension on a Buehler polishing pad, rinsed, and dried under ultra-high purity N_2 (less than 1 ppb of oxygen, CO, CO_2, and moisture). After preparation the GC electrodes were used as working electrodes in a variety of three-electrode cell configurations some of which utilized different reference electrodes. That is why the description of each experiment states the reference electrodes but for the sake of simplicity and comparability all potentials are reported versus standard hydrogen electrode (SHE).

2.2 Cu and Ag seeding

Cu nuclei were electrodeposited on GC surfaces using a Cu/Cu^{2+} pseudo reference electrode (PRE, ~0.300 V), a phosphorized Cu counter electrode (CE) by a potential pulse from open circuit potential to −0.100 V for 0.2 s in a bath containing 0.26 M $CuSO_4$ (Aldrich, 99.995 %) + 2 M H_2SO_4 GFS Chemicals, 96.0 %). Ag nuclei were electrodeposited on GC surfaces by a potential pulse from open circuit potential to −0.140 V for 5 s in 20 mM $AgClO_4$ (GFS Chemicals, 99.995 %) + 1 M $Na_2S_2O_3$ (Alfa Aesar, 99+ %) using Ag/Ag^+ PRE (~0.540 V) and a Pt CE. The seeded GC electrodes were rinsed with Barnstead Nanopure® water.

2.3 Pd and Au seeding

The Pd seeding followed a well-established two-step process [25] in which the first step, sensitization, involved immersing the GC electrode in solutions containing Sn^{2+} ions. This was followed by the nucleation step in which the sensitized GC electrodes were immersed in solutions containing Pd(II) or Au(III) chloride complexes, leading to reduction of the central ions to elemental Pd and Au on the GC surface, respectively. For these purposes solutions of 10 mM $SnCl_2$ (GFS Chemicals, 98 %) + 0.1 M HCl (JT Baker, 37.2 %), 10 mM $(NH_4)_2PdCl_4$ (GFS Chemicals, 99.999 %) + 0.1 M HCl, and 10 mM $NaAuCl_4$ (Alfa Aesar, 99.99 %) + 0.1 M HCl were prepared. Freshly polished GC electrodes used later as substrates for $Au_xAg_{(1-x)}$ alloy electrodeposition were sensitized and activated (two-step process) by immersion in $SnCl_2$/HCl for 2 min and then after rinsing in Barnstead Nanopure® water, subjected to either $(NH_4)_2PdCl_4$/HCl or $NaAuCl_4$/HCl solutions, respectively. The activated accordingly GC surfaces were then dried under N_2 gas and used immediately as substrates for $Au_xAg_{(1-x)}$ deposition. In some cases, the activation step was immediately followed by removal of the excess Sn^{4+} ions from the surface by submerging freshly deposited Pd or Au layers in 10 % HCl solubilizing solution for 3 min. Finally, the seeded GC electrodes were rinsed with Barnstead Nanopure® water and were the moved to the alloy deposition cell.

2.4 Ag–Au alloy deposition

$Au_xAg_{(1-x)}$ thin-film alloys were electrochemically deposited using a Princeton Applied Research Model 173 Potentiostat/Galvanostat with a Model 276 Interface and Model 270/250 Research Electrochemistry Software 4.00 from solutions containing Ag–Au molar ratios of 3:2, and 2:1 in 0.1 M $Na_2S_2O_3$ (Alfa AESAR, 99+ %) on GC working electrodes. Normally deposited alloys from these solutions feature 70:30 and 78:22 at.% ratios, respectively, as listed specifically for the latter composition in Table 1. Following established characterization routines the composition of these alloys was determined by energy dispersive X-ray spectroscopy (EDS) and the critical potential, E_c, was measured by analysis of anodic polarization curves [4, 5]. Exploiting the solubility of Au(I) and Ag(I) thiosulfate complexes [26, 27], Au(I)Cl complex served as source of Au^+ cations and $AgClO_4$ provided the Ag^+ cations. All solutions were prepared fresh to prevent effects associated with spontaneous metal reduction. The alloys were electrodeposited on GCs in open to the ambient environment three-electrode cell at constant potential of 0.100 V (SHE) using Ag/Ag^+ PRE ($\sim$0.500 V, SHE) and a Pt CE. The amount of the deposited alloy was controlled via current integration to charge. Identical amount of deposited alloy with a given composition for all samples was ensured through determination of the deposition efficiency calculated as the ratio of charge of de-alloyed Ag (see next step) to the total deposition charge (fixed at 200 mC cm^{-2} in all experiments). All current density values reported in this work are related to the geometric area of the electrodes used. Samples were rinsed with Barnstead Nanopure® water after the alloy deposition and SEM characterization was used to examine the density of the deposits.

2.5 The de-alloying process

The Ag was oxidatively removed by de-alloying [28] using 0.5 mM $AgClO_4$ (GFS Chemicals, 99.995 %) in 50 mM $HClO_4$ (GFS Chemicals, 70 % redistilled) employing the workstation described in the previous section. De-alloying was performed in a three-electrode cell with Ag/Ag^+ pseudo reference electrode ($\sim$0.500 V, SHE) and a Pt CE. For determination of the de-alloying critical potential [28], the applied potential was scanned from 0.500 to 1.300 V at a sweep rate of 0.2 mV s^{-1}. The anodic polarization curves were used for determining the total charge of de-alloyed Ag that in turn was included in the deposition efficiency calculation. The experimental target (accuracy of 95 %) for 2:1 Ag–Au alloy was determined to have a charge density equal to 15 mC cm^{-2}. Assuming for simplicity the deposition process to yield a flat and continuous deposit, such charge density would correspond to about 25 nm thickness of the deposited layer. After the de-alloying process the samples were thoroughly rinsed with Barnstead Nanopure® and Pb UPD was used for surface area measurements [23].

2.6 Surface area measurements-Pb UPD

Surface area measurements by Pb UPD [23] were performed in a solution containing 0.1 M $NaClO_4$ (Sigma, 99.95 %), 3 mM $Pb(ClO_4)_2$ (Aldrich, 99.995 %), and 0.01 M $HClO_4$ (GFS Chemical, 70 % redistilled). The approach relies on Pb UPD formation and/or stripping charge measurements and further normalization with the same charge(s) measured on flat samples of the same material (Au in the case of interest) thereby allowing for determination of the roughness factor of all samples. The potential was scanned from 0.400 to −0.210 V (SHE) at 10 mV s^{-1} versus Pb/Pb^{2+} PRE ($\sim$−0.200 V, SHE). H UPD was performed on the surface of platinized electrodes in identical manner scanning the potential from +0.400 to −0.680 V at 50 mV s^{-1} versus Hg/Hg_2SO_4 reference electrode [MSE ($\sim$0.650 V, SHE)] in a 0.5 M H_2SO_4 solution (GFS Chemical, 96.0 %). The platinization of all electrodes was done by 1–2 nm thick Pt layer deposited by surface limited redox replacement (SLRR) of Pb UPD following a strategy described thoroughly in our previous work [4]. All solutions were purged with ultra-

Table 1 Critical potentials E_c (V) of de-alloyed 2:1 Ag:Au thin films on different substrates

Substrate	Ag:Au ratio—solution, M and (alloy, at.%)	E_c (V) vs. SHE
Cu-seeded GC	2:1 (78:22)	0.540
Ag-seeded GC	2:1 (78:22)	0.770
Pd-seeded GC	2:1 (78:22)	0.593
Pd-seeded GC, *HCl accelerator*	2:1 (78:22)	0.823
Au-seeded GC	2:1 (78:22)	0.576
Au-seeded GC, *HCl accelerator*	2:1 (78:22)	0.823
Unseeded GC	2:1 (78:22)	0.830
Polycrystalline Au	2:1 (78:22)	0.823

high purity N_2 for at least 20 min prior to the measurements. Pt wire was used as CE.

2.7 Scanning electron microscopy and energy dispersive X-ray spectroscopy

SEM was performed for morphological characterization while the alloy composition was confirmed by EDS using a FEG-SEM Zeiss Supra 55 VP coupled with a through-the-lens detector at an accelerating voltage of 8–10 kV for imaging at magnifications as high as 200,000 times. The working distance was varied depending on the nature of the sample.

3 Results and discussion

3.1 Seeding of glassy carbon electrodes

3.1.1 Seeding of GC with Cu and Ag

Our previous works demonstrated that successful metallization of GC electrodes with Ag–Au alloy could be carried out by conventional electrodeposition [4, 5]. However, consistently with our previous work [4] the deposits consisted of isolated and somewhat polydisperse alloy clusters as shown in Fig. 1. These clusters accumulate substantial amount of material as preferential growth sites right after their nucleation. Thus, instead of developing surface area "laterally" and spreading the material in very thin layer with more points of contact to the substrate, the as-deposited clusters of big size and mass in that case have lower odds for sustaining subsequent procedures like de-alloying, functionalization with catalytically active metal (Pt, Pt–Cu) and testing (in formic acid oxidation process). Since the aim of this work has been to improve the nucleation density and hence facilitate cluster coalescence, at substantially lower deposit thickness then that realized on plain and untreated GC electrode, the use of well-known deposition protocols for seeding purposes is desirable. As mentioned in the Sect. 2, identical amount of alloy material with given composition equivalent to a 25 nm thick layer was guaranteed by studying the deposition efficiency and targeting identical charge density of the de-alloyed Ag (15 mC cm^{-2} for 2:1 Ag–Au alloy) in all deposits. This consistent layer thickness allows for meaningful comparison between all deposited layers. Seeding was first attempted by pulse electrodeposition of Cu and Ag seeds. Cu and Ag electrodeposition on GC electrodes [29–31] and other related substrates [32] has been widely studied. In this work we have chosen to use a Cu^{2+} ion containing solution that has been widely used for Cu plating in the electronics industry [33]. The deposit was created by application of short time pulses tuned to generate nanosized clusters ensembles similar to those in [31] where ammoniacal solutions containing Cu^{2+} ions are used. Ag metal nuclei were electrodeposited on GC electrodes by potential pulses generally adopting the strategy developed in [34] for nucleation of Ag clusters on GC electrodes as described in the Sect. 2. According to the cited references, the employed nucleation and growth of Cu and Ag on the GC is believed to take place via three-dimensional (3D) mode [30, 34–36]. The current time transients in the seeding process (not shown) featured current that reaches maximum, hinting first at nucleation of Cu and Ag, followed by subsequent diffusion-limited 3D growth [6]. Figures 2 and 3 present SEM characterization images of 2:1 Ag–Au alloy deposits on GC electrodes that were seeded with Cu and Ag clusters labeled in the rest of this paper as Ag–Au/Cu-GC and Ag–Au/Ag-GC, respectively. Both images feature spherical particles that while still isolated are clearly smaller and closer than those depicted in Fig. 1. The results shown in Figs. 2 and 3 represent some improvement in the targeted direction as compared to the unseeded GC surface. In both images the clusters are smaller, less separated, and more uniform in size, especially the Ag–Au/Cu-GC sample. At the same time the densification is clearly insufficient and apparently more efficient seeding treatment is needed for achieving the desired continuity of the alloy deposit at minimum thickness.

3.1.2 Seeding of GC with Pd and Au

The metallization in this section involved electroless seeding with Pd and Au clusters through a redox exchange with pre-adsorbed Sn^{2+} ions. While pulse potential strategies have been studied as an option for nucleating Pd cluster ensembles [37] we resorted in our work to the electroless approach as it is known to result in higher nucleation density compared to other ways of seeding [38]. To that end a two-step process was carried out utilizing

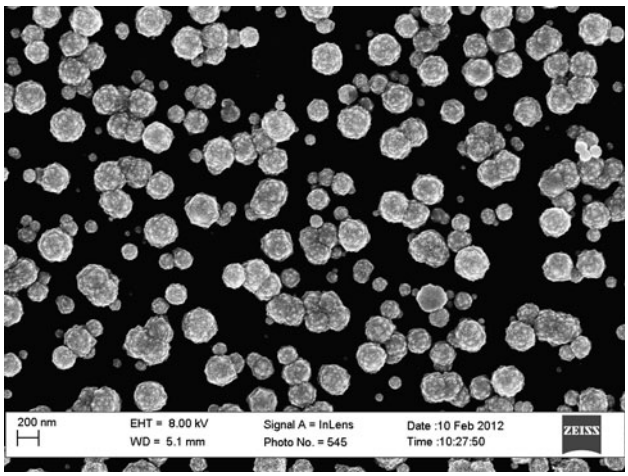

Fig. 1 FE SEM image of a de-alloyed 2:1 (78:22 at.%) Ag:Au thin film deposited originally on unseeded GC electrode (Ag–Au/GC)

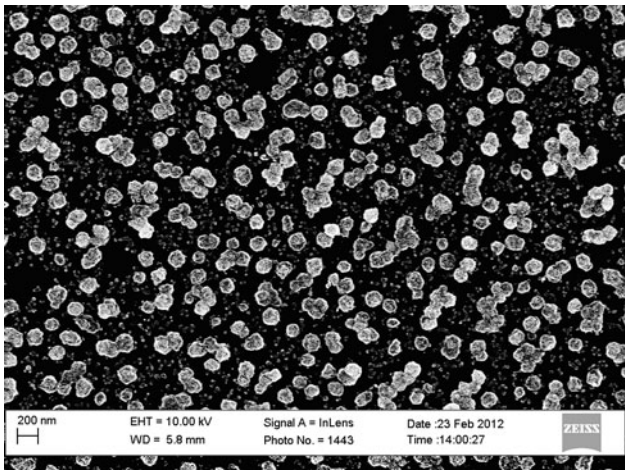

Fig. 2 FE SEM image of a de-alloyed 2:1 (78:22 at.%) Ag:Au thin film deposited originally on a Cu-seeded GC (Ag–Au/Cu-GC)

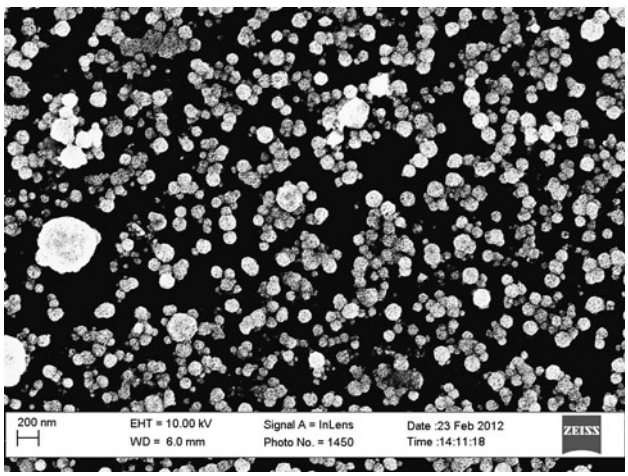

Fig. 3 FE SEM image of a de-alloyed 2:1 (78:22 at.%) Ag:Au thin film deposited originally on a Ag-seeded GC (Ag–Au/Ag-GC)

Sn^{2+} adsorption (sensitization) and Pd^{2+}–Sn^{2+} redox exchange (activation) preformed in separate baths. This cluster densification in the case of our interest facilitates eventually the particle coalescence at lower deposit thicknesses. The two-step process is cost-effective since very little Pd is used. In our study GC electrodes were sensitized by immersion in an acidic $SnCl_2$ solution followed by activation through immersion in an acidic solution of $PdCl_2$. In this work we present for the first time an alternative seeding approach in which the activation step leads to nucleation of Au clusters realized in $NaAuCl_4$ solution. The nucleation of elemental Pd and Au clusters on the GC electrode is achieved by the redox reaction that takes place between the Pd^{2+} or Au^{3+} ions in the solution and the pre-adsorbed Sn^{2+} ions from the sensitization step, as follows:

$$Sn^{2+} + Pd^{2+} \rightarrow Sn^{4+} + Pd^{0}(2e^{-}\text{exchange}) \quad (1)$$

$$3Sn^{2+} + 2Au^{3+} \rightarrow 3Sn^{4+} + 2Au^{0}(6e^{-}\text{exchange}) \quad (2)$$

An accelerator such as NaOH, EDTA, or HCl is needed in most cases in order to increase the nucleation rate in the activation step and remove the excess unreacted Sn^{2+} species from the substrate surface. The type of accelerator used also dictates the uniformity of the metal deposit. This is demonstrated by studies performed on copper in which the use of NaOH and EDTA accelerators resulted in uniform copper deposits [39]. That is why, a part of our work utilizes 10 % HCl solution [40, 41] as the accelerator and the results are compared with those obtained in the absence of accelerator. Eventually, obtained with or without accelerator, then small clusters (seed) of Pd and Au atoms nucleated in the activation process function as nucleation sites for the subsequent Ag–Au alloy deposition.

Similarly to the seeding with Cu and Ag, Figs. 4 and 5 show SEM images of 2:1 Ag:Au alloy deposits on Pd- and Au-seeded GC electrodes and labeled for future reference as Ag–Au/Pd-GC and Ag–Au/Au-GC, respectively. Both deposits contain the same amount of material as the previous samples, and no HCl accelerator is used in those deposition events. Both images feature spherical particles that are considerably smaller in comparison with the layers presented in Figs. 1, 2, and 3 and show deposited alloy being distributed more uniformly into a denser deposit. From Fig. 4, it can be deduced that metalizing the GCs with the $SnCl_2$–$NaAuCl_4$ system improves the nucleation density and that the spherical particles are evenly distributed throughout the surface. Also, while somewhat polydisperse, the alloy clusters are smaller and denser on average than those seen on Ag–Au/Cu-GC and Ag–Au/Ag-GC. From Fig. 5, it can be concluded that metallization using the $SnCl_2$–$PdCl_4$ system results in the smallest

spherical particles that grow in dense clusters leaving small areas of the surface uncovered, likely yet by the seeding process. It is also obvious that the overlapping clusters in that case are satisfactorily monodisperse and appear to be consistently smaller than those in Ag–Au/Au-GC samples. The variation in the surface coverage may be due to possible differences in the rates of exchange between the Au^{3+} ion and Sn^{2+} ions compared to the rates between Pd^{2+} and Sn^{2+}. This difference in exchange is associated with the difference in size of the ions and/or the difference in the nucleation mechanisms. It needs to be noted that the results of seeding with Au and Pd presented in this work are obtained for pre-optimized exposure time of the GC electrodes in both, the sensitization and activation processes. This study identified 2 min sensitization time as sufficient for further growth of a uniform deposit and hinted at issues associated with excess adsorption of difficult to remove Sn^{2+} ions at longer exposures. In addition, variation of the activation times in Pd–Sn^{2+} and Au–Sn^{2+} exchange reactions suggested that overall activation duration of 4 min was optimal for growing a network of overlapping clusters. Shorter times resulted in lower deposit density and prolonged exposure to the activation solution led to larger Au nuclei that impacted noticeably the Ag–Au ratio of the alloying layers in deposited in the next step. Finally, owing to the lack of literature data on Au–Sn^{2+} redox exchange reaction, Pb UPD characterization measurements [23] were performed before and right after Au activation (Fig. 6) to validate and ascertain the general feasibility of Au seeding. The cyclic voltammetry (CV) curve obtained after seeding (solid line) featured all characteristic peaks for Pb UPD on polycrystalline Au surface.

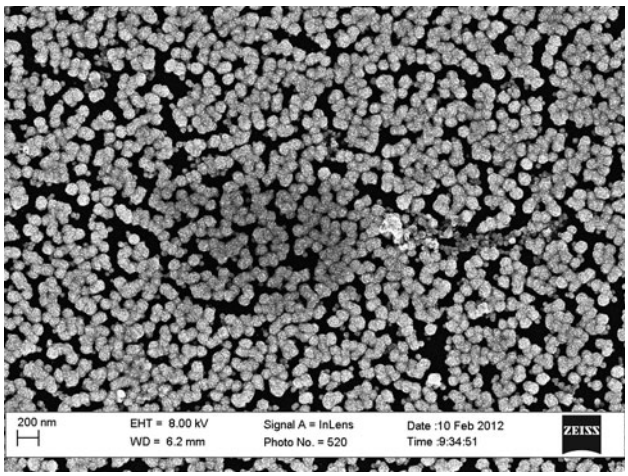

Fig. 4 FE SEM image of de-alloyed 2:1 (78:22 at.%) Ag:Au thin film deposited originally on a Au-seeded GC without accelerator used (Ag–Au/Au-GC)

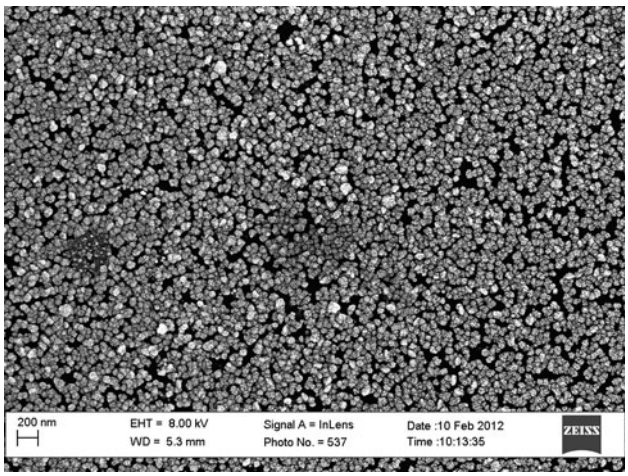

Fig. 5 FE SEM image of de-alloyed 2:1 (78:22 at.%) Ag:Au thin film deposited originally on a Pd-seeded GC without accelerator used (Ag–Au/Pd-GC)

3.2 Ag–Au Alloy deposition

3.2.1 Deposition on Cu- and Ag-seeded GCs

In our previous work [4], $Au_xAg_{(1-x)}$ thin films were deposited from a 0.1 M $Na_2S_2O_3$ bath containing varying molar ratios of Ag and Au. Unlike in that work [4] where the Au source was Au(I)Cl and the Ag source was $AgClO_4$, the present work used Au(I) and Ag(I) thiosulfate complexes directly including $Na_2S_2O_3$ as background electrolyte for the alloy deposition solution. Therefore $Au_xAg_{(1-x)}$ thin films were electrodeposited from more stable and durable solutions on GC electrodes metalized with Cu and Ag as well as on unseeded GC at a potential of 0.100 V (SHE), from baths with different molar ratios of Ag and Au in 0.1 M $Na_2S_2O_3$ solution. The seeded GC electrodes were transferred to the deposition cell with a droplet of remaining rinsing water immediately after the seeding process. This was done to prevent surface oxidation of the Ag and Cu seeds that eventually would contribute abnormally high reduction current densities during the course of alloy deposition. Also, the deposition process was initiated immediately establishing contact (by a meniscus) between the seeded electrode surface and the deposition electrolyte. Figure 7 illustrates electrodeposition of 2:1 Ag:Au alloy on Cu- and Ag-seeded GC electrodes, respectively. In Fig. 7, the deposition current density on Cu-seeded GC reaches steady state much faster than that of the Ag-seeded GC. Discussing this phenomenology one needs to take into account the difference in catalytic activities of Cu and Ag with respect to the oxygen reduction reaction (ORR). It is known that ORR on Cu takes place as a $4e^-$ process [42] while the same reaction on Ag is impeded and proceeds through an intermediate resulting in a $2e^-$ reduction process [43]. This leads to the overall higher magnitude of the current density registered on Cu-

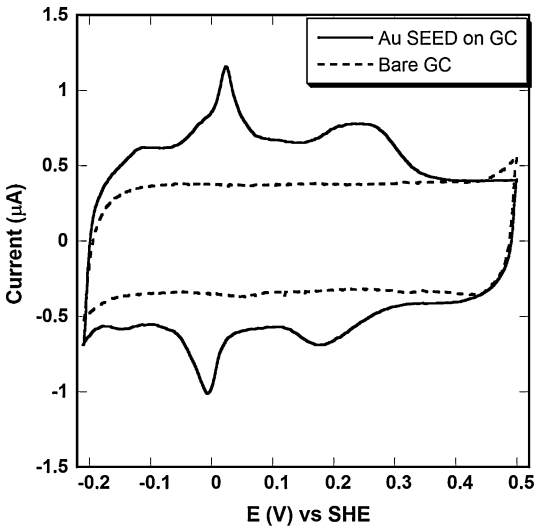

Fig. 6 CV curves showing Pb UPD on GC surface before and after Au seeding performed at 2 min sensitization and 4 min activation time. Solution: 0.1 M $NaClO_4$ + 0.003 mM $Pb(ClO_4)_2$ + 0.01 M $HClO_4$. Scan rate: 10 mV s^{-1}

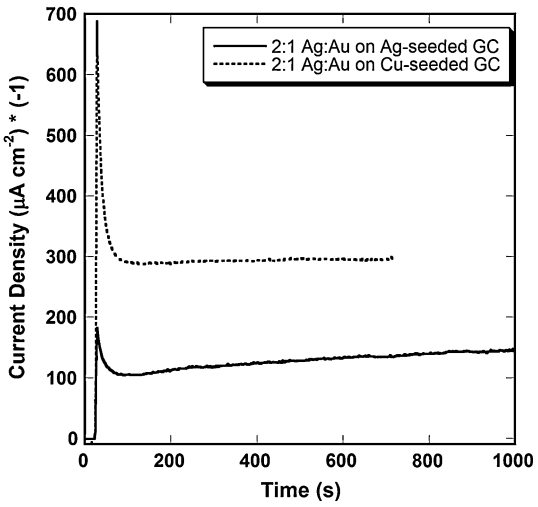

Fig. 7 Chronoamperogram of 2:1 (78:22 at.%) Ag:Au thin film deposition on Cu- and Ag-seeded GC. Solution containing Ag(I):Au(I) molar ratio of 2:1 in 0.1 M $Na_2S_2O_3$. Deposition potential: 0.100 V (SHE)

seeded GC compared to the Ag-seeded one. Indeed, it is not surprising to observe faster establishment of steady-state current on the Cu-seeded sample as a large portion of the current is attributed to the competitive ORR. It is known that the diffusion-limited ORR depends on particle size and distribution, only before the semi-infinite diffusion profile is developed and a steady-state current is established [44]. Thus, in the realm of established diffusion limitation the total current comprises the contribution of both competing reactions. In concert with this result, a close inspection of Fig. 2 shows the presence of bi-modal distribution of cluster sizes indicating that the smaller clusters are most likely Cu carrying out ORR and the larger ones carrying the alloy deposition. Overall, the Cu-seeded GC seems to feature two major length scales that are individually uniform. At the same time the significantly lower and steadily increasing current density in Fig. 7 and the size-uniform clusters deposited on Ag-seeded GC suggest considerably lower (or lack of) ORR activity. This boosts the contribution of the deposition process only, and ultimately results in surface area evolution manifested by steadily increasing magnitude of the deposition current.

3.2.2 *Thin-film alloy deposition for Pd- and Au-seeded GCs*

$Au_xAg_{(1-x)}$ thin films were electrodeposited on GCs catalyzed with Pd and Au and at a potential of 0.100 V versus SHE from baths comprising different molar ratios of Ag and Au in 0.1 M $Na_2S_2O_3$ solution. The GC electrodes seeded with Au and Pd were used immediately as it was found that prolonged exposure to the atmosphere introduces uncertainties into the alloy deposition process associated with possible passivation of the seed with ambient contamination prone to adsorption on Au and Pd surfaces. Figure 8 shows chronoamperograms of 2:1 Ag–Au alloy deposition on Pd- and Au-seeded GCs, respectively. The current quickly reached steady state, indicating that the GC surface is free of impurities and also that the catalytic nuclei on the surface were uniformly distributed. It is clear from Fig. 8 that a phenomenology similar to that described in the previous section impacts the Ag–Au/Pd-GC and Ag–Au/Au-GC synthesis. More specifically, the Pd-seeded samples feature substantially higher current density compared to the Au-seeded ones. This is a result of the well-known ability of Pd to serve as one of the best catalysts for ORR [45]. A large portion of the current can be attributed to ORR on Pd-seeded following arguments similar to those previously described and interpreted for the case of Cu-seeded GC samples. The results obtained on Au-seeded GC samples do not support this phenomenology, which is not surprising given the relative passivity of Au toward ORR in acidic media [46]. With these effects taken into account, a remarkable achievement is the higher cluster density and considerably smaller cluster size in the case of Ag–Au/Pd-GC and Ag–Au/Au-GC samples in comparison with the unseeded GC electrodes (Figs. 1, 4, and 5). Also, the comparison of Figs 1 and 4 along with the Pb UPD characterization of Au-seeded GC surface (Fig. 6) clearly validates the applied for the first time Au activation approach as alternative of the Pd-based one. The best results presented by clusters grown uniformly to reach a status that is close to coalescence are obtained for Ag–Au/Pd-GC samples despite the ORR activity documented to take place along with alloy deposition. Alloy deposition of lower thicknesses (based on 8, 12, and 20 mC cm^{-2} charge density of de-

alloyed Ag) were also performed in order to assess which deposition thickness would provide the most uniform and complete surface coverage. It was concluded that the overall decrease in thickness led to insufficient cluster coverage whereas higher thickness often caused delamination of the alloy from the GC electrode.

3.3 De-alloying behavior

3.3.1 De-alloying behavior of Ag–Au/Cu-GC and Ag–Au/Ag-GC samples

The selective dissolution of Ag (de-alloying) from the 2:1 Ag–Au/Cu-GC and Ag–Au/Ag-GC thin films was performed using a procedure described in detail in the Sect. 2. Figure 9 illustrates anodic polarization curves of the Ag–Au alloy samples. Presented for comparison are also results from the de-alloying of same composition Ag–Au alloys deposited on a plain Au substrate as well as an anodic polarization curve on bare GC electrode (to set the baseline). Special attention in the analysis of the polarization curves has been on the de-alloying critical potential [28] that similarly to our previous work has been approximated with the potential at which the main dissolution process is initiated [5]. This coincides with the onset of the major anodic peak in each polarization curve. As shown in Table 1 the anodic polarization curves obtained by de-alloying 2:1 Ag–Au/Cu-GC and Ag–Au/Ag-GC thin films featured critical potentials of 0.54 and 0.770 V, respectively. The NPG obtained from de-alloying the 2:1 Ag–Au thin films on unseeded GC and Au substrates featured very close critical potentials of 0.810 and 0.823 V, respectively.

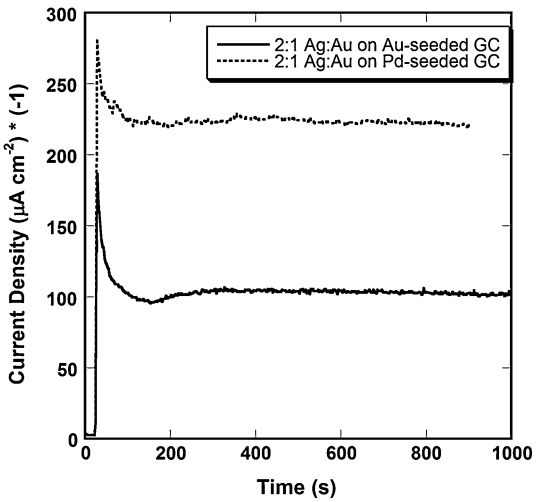

Fig. 8 Chronoamperogram of 2:1 (78:22 at.%) Ag:Au thin film deposition on Au- and Pd-seeded GC. Solution containing Ag(I):Au(I) molar ratio of 2:1 in 0.1 M $Na_2S_2O_3$. Deposition potential: 0.100 V (SHE)

The difference of about 0.015 V in the latter case is generally expected as the curved particle surfaces of the alloy on GC are known to de-alloy slightly easier [5]. It is worthwhile to note that the critical potentials of the Ag–Au/Cu-GC and Ag–Au/Ag-GC thin films are far more negative than those of the unseeded GC and Au substrates, which is most likely due to the seeding metal's impact on the composition and/or structure of the accordingly deposited Ag–Au alloys. Unexpectedly and interestingly enough, the Ag–Au/Cu-GC sample shows virtually no critical potential behavior upon de-alloying. The major (qualitative) difference between Cu-seeded samples and unseeded samples could be associated with possible alloying between the Cu and Au that are known as metals with a very strong affinity to each other [47]. Such alloying is known and documented even in ultra-high vacuum deposition [48] in systems like Au/Ni(110) [49] and Pd/Cu(100) [50] that feature very high surface dynamics. Such alloying would substantially decrease the strength of interaction between Au and Ag and in turn leave most of the Ag atoms in the deposit as free and/or very weakly bonded instead of forming a conventional single-phase Ag–Au alloy. Therefore, during the de-alloying process, the weakly bonded Ag would de-alloy at potentials that are close to the dissolution (oxidation) potential of elemental Ag. Once the process is initiated, Cu is also believed to participate in the mass-stripping process weakening the bond between particles and GC substrate. As per Ag–Au/Ag-GC alloys, the Ag seed could change the intended Ag:Au mole ratios generally leading to deposition of depleted in Au alloys. This would result in stripping of higher fraction of Ag than anticipated which is manifested during de-alloying through the negative shift in the critical potential. This expectation is justified by the fact that alloys with a higher ratio of the less noble component tend to exhibit more negative critical potentials [28]. In another scenario, if there are still free/unbonded Ag clusters on the GC surface that for some reason did not nucleate Ag–Au alloy, these free nuclei would dissolve (oxidize) similarly to elemental Ag leading eventually to far more negative critical potentials. All of the above possibilities along with the immediate contact of "dissolution-prone" pure Ag clusters with the GC surface could generally destabilize the alloy deposit and could eventually trigger delamination of the NPG resulting from the de-alloying process. This was confirmed by a considerable degree of failure of the scotch tape test by NPG samples deposited on Cu- and Ag-seeded GC electrodes.

3.3.2 De-alloying behavior of Ag–Au/Pd-GC and Ag–Au/Au-GC samples

The de-alloying of Ag–Au/Pd-GC and Ag–Au/Au-GC electrodes (synthesized with and without HCl accelerator)

is presented in Fig. 10 where a comparison is also made with the behavior of unseeded Ag–Au/GC and Ag–Au/Au samples. Also an anodic polarization curve obtained on Pd-seeded sample without any alloy on it is presented in Fig. 10 for comparison (and to set the baseline). As shown in Fig. 10 and in Table 1, the Ag–Au/Pd-GC and Ag–Au/Au-GC electrodes synthesized without use of HCl as accelerator feature multi-step de-alloying with onset of bulk dissolution at 0.576 and 0.593 V, respectively. These values are very negative and in neither of these cases could be explained by conventional de-alloying arguments involving the anticipated alloy constituents and any of the seed metals (Au or Pd). Given the nature of the Au and Pd seeding processes, the only plausible explanation in both cases could be associated with the presence of excess Sn^{2+} used as sensitizing agent after the activation (redox exchange) process. Should the unreacted Sn^{2+} still be on the surface when the alloy deposition process is initiated, the deposition potential would be negative enough to co-deposit elemental Sn along with the Ag and Au. In such a case effects similar to the ones described in the previous section for Cu-seeded samples could become critical in governing the overall processing phenomenology. More specifically, unlike with Ag, Sn is known to readily form with Au multiple stable intermetallic compounds [51] and thus the excess Sn^{2+} could play the "third element" role in the alloy deposition process impacting the strength of bonding between Ag and Au. In an effort to address this issue and create the best conditions for the excess Sn^{2+} removal, 10 % HCl solution was employed as an accelerator immediately following the Au and Pd seeding processes. The 2:1 Ag:Au alloys were then deposited on the seeded GCs and upon completion of the growth, de-alloying was carried out. As shown in Fig. 10 and Table 1, the polarization curves and critical potentials of accordingly processed samples were close to those obtained from de-alloyed 2:1 Ag:Au alloys on unseeded GC and Au substrates. In addition to that, the anodic polarization curves are virtually identical with those obtained on unseeded GC and Au substrate, featuring critical potentials in the range 0.820–0.825 V in both cases. These results suggest that the acceleration step involving removal of Sn^{2+} remnants is essential in improving the overall synthetic route and in minimizing the impact of side effects related to the seeding process on the structure, morphology, and continuity of the developed NPM layers.

3.4 Surface area measurements

3.4.1 Surface area measurements of Ag–Au/Cu-GC and Ag–Au/Ag-GC samples

One of the main points of interest in this work was the development of stable NPG samples featuring tunable porosity length scale. The porosity leading to highly developed surface area would make these deposits excellent candidates for application in catalysis. Surface area measurements were carried out using the Pb UPD approach developed in previous work of our group [23]. A confirmation of the surface area measurements was provided by separately performed H UPD on NPG samples coated with 1–2 nm Pt thin film following a procedure described in detail in the Sect. 2 and employed earlier elsewhere as well [4]. The comparison between both UPD approaches yielded no more than 5 % difference. An illustration for typical surface area measurement is presented in Fig. 11 comparing the area of the NPG sample developing after the de-

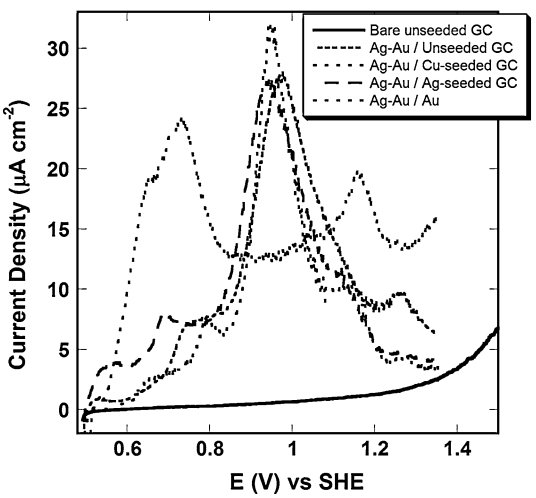

Fig. 9 Anodic polarization curves of de-alloyed 2:1 (78:22 at.%) Ag:Au thin films on different substrates (see legend). Solution: 0.5 mM $AgClO_4$ + 50 mM $HClO_4$. Scan rate: 0.2 mV s^{-1}

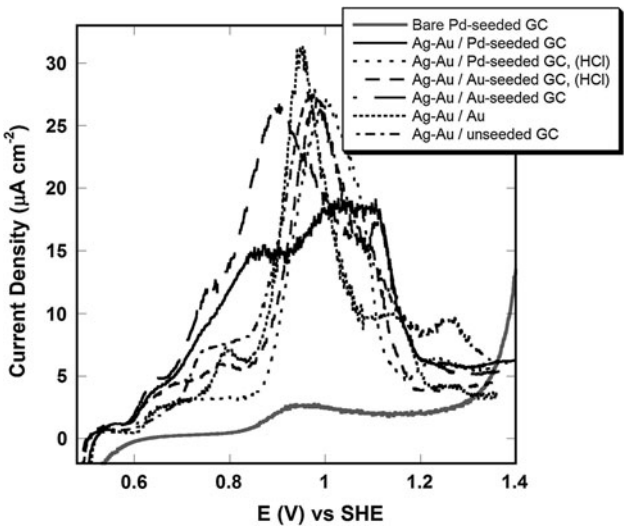

Fig. 10 Anodic polarization curves of de-alloyed 2:1 (78:22 at.%) Ag:Au thin films on different substrates (see legend). Solution: 0.5 mM $AgClO_4$ + 50 mM $HClO_4$. Scan rate: 0.2 mV s^{-1}

alloying process with one of the as-deposited 2:1 Ag–Au/Ag-GC samples. The ratio of both surface areas defines the roughness factor, summarized in Table 2 for all type of approaches entertained in this work. The inset presents a H UPD curve on the same sample after platinization (Pt-NPG). Analysis of those results suggests that Ag–Au/Cu-GC electrodes feature consistently low surface roughness factor of 0.54 due to the loss of material during de-alloying and coarsening of the de-alloyed structure. This result is expected given the lack of typical de-alloying behavior discussed in the previous section and manifested by the absence of critical potential. Unlike the case of Cu seeding, Ag–Au/Ag-GC samples featured a roughness factor of 3.82 and seemed to be substantially better suited for further processing and testing. This is confirmed even by visual inspection of Fig. 11 where the area under the Pb UPD curve registered after de-alloying is considerably higher compared to the one obtained on as-electrodeposited alloy sample.

3.4.2 *Surface area measurements for Ag–Au/Au-GC and Ag–Au/Pd-GC samples*

The analysis of surface area development on Ag–Au/Au-GC and Ag–Au/Pd-GC electrodes clearly demonstrates trends that unambiguously manifested themselves through the polarization curves shown in Fig. 10. We speculated already that Ag–Au/Au-GC and Ag–Au/Pd-GC electrodes had excess of Sn^{2+} that incorporates and alloys through the course of the deposition process, thereby playing the role of the "third element" suspected to destabilize the bonding between Ag and Au. This in general would result in inefficient de-alloying and low surface area development. According to that argument, it is evident from Table 2 that GC samples that had been seeded via the two-step process involving Sn^{2+} ions had relatively low surface area development and respectively low roughness factors of 1.80 for the Ag–Au/Pd-GC and 1.73 for the Ag–Au/Au-GC, respectively. In line with our earlier discussion the results summarized in Table 2 also suggest that the HCl accelerator helps achieve de-alloying behavior leading to systematically higher values of the roughness factors of 2.92 and 3.08, respectively. This constitutes an increase by about a factor of 2 that given the low overall thickness of the seeded layers is a considerable area development. The area increase on Ag–Au/Au-GC and Ag–Au/Pd-GC samples compares reasonably well to control samples where NPG was processed on unseeded GC and pure Au substrates (roughness factors of 3.2 and 3.1, respectively). Therefore, one can conclude the use of accelerator facilitates the development of the largest possible surface area in seeded samples featuring substantially smaller clusters and remarkably higher cluster density. This overall set of properties provides a great deal of structural improvement and renders Ag–Au/Au-GC and Ag–Au/Pd-GC layers nearly continuous. Indeed, more work is needed on the details of surface area development and its implication to the properties of catalysts processed according to the proposed strategies for enhanced nucleation density. Results of detailed application tests will be presented in a future work of our group.

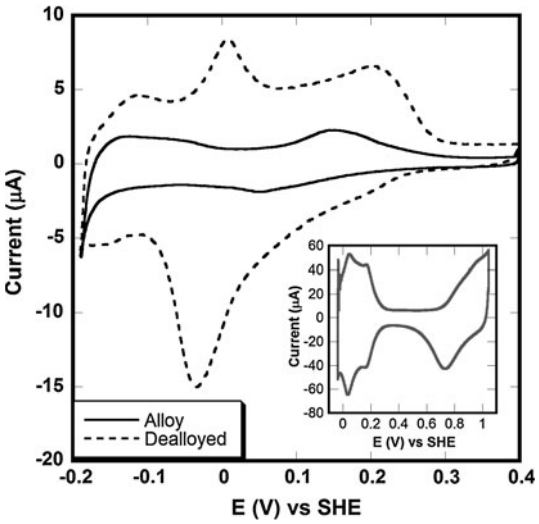

Fig. 11 CV curves showing Pb UPD before and after de-alloying carried out on 2:1 (78:28 at.%) Ag–Au/Ag-GC. Solution: 0.1 M $NaClO_4$ + 0.003 mM $Pb(ClO_4)_2$ + 0.01 M $HClO_4$. Scan rate: 10 mV s^{-1}. The *inset* depicts a CV curve of H UPD performed in 0.5 M H_2SO_4 at a scan rate of 50 mV s^{-1} on NPG same sample after platinization

Table 2 Surface area measurements before and after de-alloying of 2:1 Ag:Au on different substrates

Substrate	Ag:Au ratio—solution, M and (alloy, at.%)	Before de-alloying (cm^2)	After de-alloying (cm^2)	Roughness factor
Cu-seeded GC	2:1 (78:22)	0.94	0.51	0.54
Ag-seeded GC	2:1 (78:22)	0.21	0.8	3.82
Pd-seeded GC	2:1 (78:22)	0.25	0.45	1.80
Pd-seeded GC, *HCl accelerator*	2:1 (78:22)	0.25	0.73	2.92
Au-seeded GC	2:1 (78:22)	0.33	0.57	1.73
Au-seeded GC, *HCl accelerator*	2:1 (78:22)	0.22	0.84	3.08
Unseeded GC	2:1 (78:22)	0.19	0.60	3.2
Polycrystalline Au	2:1 (78:22)	0.24	0.75	3.1

4 Conclusions

This work demonstrates that nucleation high density cluster network and eventual generation of nearly continuous Ag–Au deposit at minimum thickness on GC substrates is facilitated to different extent by seeding with Cu, Ag, Au, and Pd clusters. It has been found that seeding with Cu and Ag carried out by electrodeposition increases the nucleation density and even (in the case of Ag–Au/Ag-GC) sponsors a significant development of surface area after de-alloying. However, a major drawback of this approach is a frequently encountered complete or partial delamination of the NPG thin film upon de-alloying, leading to eventual loss of active surface area and to poor feasibility in practical application. It has been also demonstrated that enhanced nucleation density and thus processing of nearly continuous NPG layers at very low thickness on GC electrodes could be achieved by sensitization with Sn^{2+} and activation with $PdCl_2$ and/or $AuCl_3$, following common practices of electroless deposition. At the same time the application of these practices warrants the removal of the excess Sn^{2+} ions with 10 % HCl solution known also as acceleration routine. In this work the use of accelerator has been determined as critical for the achievement of a de-alloying behavior identical to that of control Ag–Au samples deposited on unseeded GC and Au electrodes. It is noteworthy that along with the seeding approaches, this work demonstrates for the first time Au activation of GC surfaces realized by redox exchange with Sn^{2+} ions. ORR has been found also to play role as a side reaction, particularly during alloy deposition on Cu- and Pd-seeded GC electrodes. The surface area development for alloys deposited on differently seeded samples is consistently in line with the observed trends in the de-alloying behavior of the respective samples. Future work is needed for revealing and assessing the implication of the developed approaches on the performance of catalysts fabricated on GC electrodes metalized with different metal seeds.

Acknowledgments The authors of this work acknowledge the financial support by the National Science Foundation, Division of Materials Research (DMR-0742016). The authors thank also Edmond Fey for the help in obtaining the SEM images.

References

1. Zhong CJ, Luo J, Fang B et al (2010) Nanostructured catalysts in fuel cells. Nanotechnology 21(6):062001–062021
2. Knupp SL, Vukmirovic MB, Haldar P et al (2010) Platinum monolayer electrocatalysts for O_2 reduction: Pt monolayer on carbon-supported PdIr nanoparticles. Electrocatalysis 1(4): 213–223
3. Guo DJ, Ding Y (2012) Porous nanostructured metals for electrocatalysis. Electroanalysis 24(11):2035–2043
4. McCurry DA, Kamundi M, Fayette M et al (2011) All electrochemical fabrication of a platinized nanoporous Au thin-film catalyst. ACS Appl Mater Interface 3(11):4459–4468
5. Kamundi M, Bromberg L, Fey E et al (2012) Impact of structure and composition on the dealloying of $Au_xAg_{(1-x)}$ alloys on the nanoscale. J Phys Chem C 116(26):14123–14133
6. Bicelli LP, Bozzini B, Mele C et al (2008) A review of nanostructural aspects of metal electrodeposition. Int J Electrochem Sci 3(4):356–408
7. Budevski E, Staikov G, Lorenz WJ (2000) Electrocrystallization nucleation and growth phenomena. Electrochim Acta 45(15–16): 2559–2574
8. Charbonnier M, Alami M, Romand M (1996) Plasma treatment process for palladium chemisorption onto polymers before electroless deposition. J Electrochem Soc 143(2):472–480
9. Charbonnier M, Alami M, Romand M (1998) Electroless plating of polymers: XPS study of the initiation mechanisms. J Appl Electrochem 28(4):449–453
10. Charbonnier M, Romand M, Goepfert Y et al (2006) Copper metallization of polymers by a palladium-free electroless process. Surf Coat Technol 200:5478–5486
11. Zhang JY, Esrom H, Boyd IW (1996) Decomposition mechanisms of thin palladium acetate film with excimer UV radiation. Appl Surf Sci 399:96–98
12. Bauer A, Ganz J, Hesse K et al (1990) Laser-assisted deposition for electronic packaging applications. Appl Surf Sci 46:113–120
13. Padiyath R, David M, Babu SV (1991) Metallized plastics 2: fundamental and applied aspects. Plenum Press, New York
14. Kim BS, Kang SY, Seo HS et al (2007) Improved nucleation behavior of Ru thin films prepared by MOCVD on $TiCl_4$ Pretreated substrates. Electrochem Solid State Lett 10(10):D113–D115
15. De Minjer CH, Boom PFJvd (1973) The nucleation with $SnCl_2$–$PdCl_2$ solutions of glass before electroless plating. J Electrochem Soc 120(12):1644–1650
16. Pearlstein F (1955) Electroless nickel deposition. Met Finish 53(8):59
17. Sun H, Sun G, Wang S et al (2005) Pd electroless plated Nafion(R) membrane for high concentration DMFCs. J Memb Sci 259:27–33
18. Kuzmik JJ (1990) Plating on plastics. In: Mallory GO, Hadju JB (eds) Electroless plating: fundamentals and applications. The American Electroplaters and Surface Finishers Society, Orlando
19. Charbonnier M, Romand M (2003) Polymer treatments for enhanced adhesion of metals deposited by the electroless process. Int J Adhes Adhes 23:277–285
20. Krause LJ, Reider JA (1987) US Patent 4710403
21. Krause LJ, Reider JA (1988) US Patent 4775556
22. Mazur S, Reich S (1986) Electrochemical growth of metal interlayers in polyimide film. J Phys Chem 90:1365–1372
23. Liu Y, Bliznakov S, Dimitrov N (2009) Comprehensive study of the application of a Pb underpotential deposition-assisted method for surface area measurement of metallic nanoporous materials. J Phys Chem C 113(8):12362–12372
24. Mayrhofer KJJ, Strmcnik D, Blizanac BB et al (2008) Measurement of oxygen reduction activities via the rotating disc electrode method: from Pt model surfaces to carbon-supported high surface area catalysts. Electrochim Acta 53(7):3181–3188
25. Schlesinger M, Paunovich M (2010) Modern electroplating (the ECS series of texts and monographs), 5th edn. Wiley, New York
26. Liew MJ, Roy S, Scott K (2003) Development of a non-toxic electrolyte for soft gold electrodeposition: an overview of work at University of Newcastle upon Tyne. Green Chem 5(4):376–381
27. Vogel AI, Svehla G (eds) (1996) Vogel's qualitative inorganic analysis, 7th edn. Addison Wesley Longman, Singapore
28. Sieradzki K, Dimitrov N, Movrin D et al (2002) The dealloying critical potential. J Electrochem Soc 149(8):B370–B377

29. Jaya S, Prasada TR, Rao GP (1986) Underpotential deposition studies of copper on glassy carbon. J Chem Sci 97(5–6):581–586
30. Bonou L, Eyraud M, Crousier J (1994) Nucleation and growth of copper on glassy carbon and steel. J Appl Electrochem 24(9): 906–910
31. Grujicic D, Pesic B (2005) Reaction and nucleation mechanisms of copper electrodeposition from ammoniacal solutions on vitreous carbon. Electrochim Acta 50(22):4426–4443
32. Vassos BH, Mark HBJ (1967) The anodic dissolution of thin films of copper metal from pyrolytic graphite: a study of the multiple dissolution current peaks. J Electroanal Chem 13:1–9
33. Liu Y, Wang J, Yin L et al (2008) Influence of plating parameters and solution chemistry on the voiding propensity at electroplated copper-solder interface. J Appl Electrochem 38(12):1695–1705
34. Lin ZB, Xie BG, Chen JS et al (2009) Nucleation mechanism of silver during electrodeposition on a glassy carbon electrode from a cyanide-free bath with 2-hydroxypyridine as a complexing agent. J Electroanal Chem 663:207–211
35. Darko G, Batric P (2002) Electrodeposition of copper: the nucleation mechanisms. Electrochim Acta 47:2901–2912
36. Barradas RG, Fletcher S, Szabo S (1977) The electro-deposition of silver on stationary and rotating glassy carbon discs. Can J Chem 55:4037–4044
37. Rezaei M, Tabaian SH, Haghshenas DF (2012) A kinetic description of Pd electrodeposition under mixed control of charge transfer and diffusion. J Electroanal Chem 687:95–101
38. Marton JP, Schlesinger M (1968) The nucleation, growth and structure of thin Ni-P films. J Electrochem Soc 115(1):16–21
39. Horkans J, Kim J, McGrath C et al (1987) J Electrochem Soc 134:300–304
40. Walter A Schubert (1973) Method of oxidizing tin and treatment. US Patent
41. Charles R Shipley Jr (1959) Method of electroless deposition on a substrate and catalyst solution therefore. US Patent
42. Vukmirovic MB, Vasiljevic N, Dimitrov N et al (2003) Diffusion-limited current density of oxygen reduction on copper. J Electrochem Soc 150(1):B10–B15
43. Kazeman I, Hasanzadeh M, Jafarian M et al (2010) Oxygen reduction reaction on a rotating Ag/GC disk electrode in acidic solution. Chin J Chem 28(4):504–508
44. Vukmirovic MB, Dimitrov N, Sieradzki K (2002) Dealloying and corrosion of Al alloy 2024-T3. J Electrochem Soc 149(9):B428–B439
45. Xiao L, Zhuang L, Liu Y et al (2009) Activating Pd by morphology tailoring for oxygen reduction. J Am Chem Soc 131(2): 602–608
46. Miah MR, Ohsaka T (2009) Kinetics of oxygen reduction reaction at tin-adatoms-modified gold electrodes in acidic media. Electrochim Acta 54(24):5871–5876
47. Mallett JJ, Shao W, Liang D et al (2009) Underpotential codeposition of Cu–Au alloys. Electrochem Solid State Lett 12(8): D57–D60
48. Basenbacher F, Nielsen LP, Sprunger PT (1997) The chemical physics of solids surfaces. In: King DA, Woodruff DP (eds) Growth and properties of ultrathin epitaxial layers, vol 8. Elsevier, Amsterdam
49. Nielsen LP, Besenbacher F, Stensgaard I et al (1995) Dealloying phase-separation during growth of Au on Ni(110). Phys Rev Lett 74(7):1159–1162
50. Murray PW, Stensgaard I, Laegsgaard E et al (1995) Mechanisms of initial alloy formation for Pd on Cu(100) studied by STM. Phys Rev B 52(20):14404–14407
51. Matijasevic GS, Lee CC, Wang CY (1993) Au–Sn alloy phase-diagram and properties related to its use as a bonding medium. Thin Solid Films 223(2):276–287